



SENSITIVITY STUDY OF NEAR-SOURCE GROUND MOTION

Brad T AAGAARD¹, John F HALL² And Thomas H HEATON³

SUMMARY

We studied the sensitivity of near-source ground motions for hypothetical events on a thrust fault (M_w 6.6 to 7.0) and a strike-slip fault (M_w 7.0 to 7.1) to five earthquake source parameters. We systematically varied the rupture speed, maximum slip rate, hypocentre location, distribution of final slip, and fault depth. We used the finite element method to discretize a homogeneous or layered half-space into an unstructured mesh to model the wave propagation in the domain surrounding the fault.

Our sensitivity study of near-source ground motion indicates it is very important to include directivity effects when modelling near-source ground motion. In the thrust fault scenarios a double velocity pulse sweeps along the surface in the direction of the propagating rupture. For most of the scenarios the peak velocity, filtered to periods longer than 2.0 sec, exceeds 1.0 m/sec over an area of 100 square kilometres. In the strike-slip scenarios a complex series of pulses involving the shear wave and Rayleigh waves propagates in the direction of the rupture with the most severe motion confined to a narrow region along the fault. The peak, filtered velocity exceeds 1.0 m/sec over an area of 700 square kilometres. We found the ground motions strongly sensitive to the material properties and fault depth, moderately sensitive to the hypocentre location, rupture speed, and maximum slip rate, and relatively insensitive to the distribution of final slip. The shape of the near-source factor, N_v , from the 1997 Uniform Building Code does not correlate with the zone of severe shaking in the case of blind thrust faults, because the maximum displacements and maximum velocities tend to occur up-dip from the top of the fault.

INTRODUCTION

The 1994 Northridge and 1995 Kobe earthquakes demonstrated that we still have much to learn about how faults rupture and the resulting ground motions. These earthquakes reminded us that even moderate events can cause substantial damage. Records from these two events significantly increased our limited knowledge of severe ground motion close to rupturing faults. However, we need more information about the robustness of the characteristics of near-source ground motion. Furthermore, while inversions of strong ground motions indicate the area where slip occurred, identify the speed of the fault rupture, and give an estimation of the maximum slip rates, they do not provide information about the sensitivity of the ground motion to variations in the source parameters. We focus on resolving these issues by computing the time histories of motion using finite element models for many hypothetical scenarios on a strike-slip fault and a shallow dipping thrust fault. Although several computationally efficient methods have been developed to synthesise ground motions on finite faults with prescribed slip in a layered half-space [Heaton, 1995], we use the finite element method because we intend to extend the software to simulations with dynamic rupture and three-dimensional material properties.

METHODOLOGY

We want to solve for the ground motion time histories governed by the three dimensional, dynamic, elasticity equation. We use the finite element method to turn the elasticity equation into a matrix differential equation.

¹ California Institute of Technology, Pasadena, USA

² California Institute of Technology, Pasadena, USA, johnhall@caltech.edu

³ California Institute of Technology, Pasadena, USA, heaton_t@caltech.edu

Most finite element texts, e.g. [Rao, 1999], provide the details of this technique. The four-sided tetrahedral finite element with four nodes allows highly variable node spacing and requires minimal storage; both are necessary for efficient modeling of domains with heterogeneous material properties [Bao et al., 1998]. We numerically integrate the matrix differential equation using the central difference method, because it requires minimal computation effort and is well suited for parallel processing. We model the ground surface as a free surface and create non-reflecting boundaries on the lateral sides and bottom of the domain. The dampers composing the non-reflecting boundaries absorb waves as they hit the boundaries which mimics the behavior of the waves continuing to propagate past the edges of the domain [Cohen, 1980].

For slip on the fault we want to impose a dislocation in the finite element model. We incorporate the fault plane into the geometry of the finite element model and give all the nodes on the fault plane double the usual number of degrees of freedom to allow one side of the fault to move relative to the other side. Each fault node has six translational degrees of freedom that are split such that each side of the fault has the typical three degrees of freedom [Aagaard, 1999]. By transforming the degrees of freedom on the fault plane to relative and average degrees of freedom, we gain explicit control of the relative motion across the fault. To prescribe the slip we simply set the displacements at the relative degrees of freedom in the slip direction at each time step in the numerical integration. For the slip time history we use the integral of Brune's far field time function, which is given by equation [1] where the slip starts at time t_0 , the final slip is D_{max} , and τ is a time constant [Brune, 1970].

$$D(t) = D_{max} (1 - \exp(-(t-t_0)/\tau))(1+(t-t_0)/\tau) \quad [1]$$

Simulations that involve hundreds of thousands to millions of degrees of freedom require hundreds of megabytes to gigabytes of memory and billions of floating point operations. Parallel computing provides a suitable environment for solving such problems by distributing both the storage and computation among many processors. We implement the software using the Message Passing Interface and C++ and run the simulations on the Intel Paragon and Hewlett Packard Exemplar supercomputers at the Center for Advanced Computing Research at the California Institute of Technology. The inertial bisection algorithm provides a fast, easy method for partitioning the unstructured meshes among the processors [Williams, 1991]. We use a global refinement procedure [Aagaard, 1999] to turn a course mesh created with Structural Dynamics Research Corporation's IDEAS into a mesh with the appropriate spatial resolution for propagation of waves with periods down to 2.0 sec.

RESULTS

We study sensitivity of near-source ground motions to variations in the earthquake source parameters with the goal of identifying the characteristics of the rupture process that most strongly influence the strong ground shaking. We systematically vary the seismic source parameters for both a strike-slip fault and a shallow dipping thrust fault. We select from four hypocentre locations (labelled HA to HD in figure 1(a) and figure 3), three maximum slip rates (1.0 m/sec, 1.5 m/sec, and 2.0 m/sec), three rupture speeds (70%, 80%, and 90% of the local shear wave speed), three to five spatial distributions of the final slip, two values of average slip, and three depths of the top of the fault (0.0 km, 4.0 km, and 8.0 km). For each parameter we generally vary the value equally about the base case, e.g. we select maximum slip rates of 2.0 m/sec and 1.0 m/sec about the base case value of 1.5 m/sec. Additionally, we compare the ground motions from a homogeneous half-space to those from a layered half-space.

Strike-Slip Fault

The geometry of the strike-slip fault roughly matches the combined fault segments that ruptured in the June 1992 Landers event. We enclose the 60 km long and 15 km wide fault in a domain 100 km long, 40 km wide, and 32 km deep as shown in figure 1(a). We impose pure right-lateral slip on the vertical fault to create earthquakes with a nominal moment magnitude of 7.0. Figure 1(b) shows the mass density, shear wave speed, and dilatational wave speed as a function of depth for the layered half-space. For the homogeneous half-space we simply use the material properties from the layered half-space at a depth of 6.0 km. After global refinement the finite element model contains six million degrees of freedom and ten million tetrahedral elements. The base case features a relatively homogeneous distribution of slip that extends to the surface and is tapered on the other three edges. We prescribe an average slip of 2.0 m, a maximum slip rate of 1.5 m/sec, a rupture speed of 80% of the local shear wave speed, and a hypocentre at location HA.

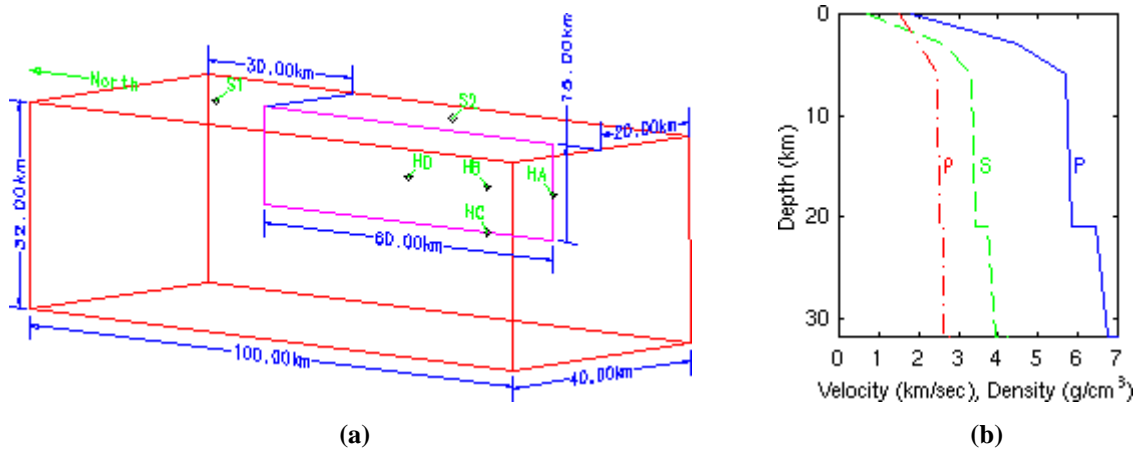


Figure 1: (a) Orthographic view of the geometry of the domain encompassing the strike-slip fault. The labels HA to HD denote the various hypocentre locations. We examine time histories at sites S1 and S2. (b) Density, shear wave speed, and dilatational wave speed as a function of depth for the layered half-space.

The earthquake simulations on the strike-slip fault share several distinct features. When slip occurs in the softer material in the top six kilometres of the domain, the rupture slows considerably in this region causing the curvature of the rupture front to increase as time progresses. This disrupts the reinforcement of the shear wave by the rupture, and the peak velocities decrease above the centre of the fault. Once the curvature is large enough, the reinforcement stabilises, and the peak velocities increase and become uniform along the strike near the north end of the fault (see figure 2). The maximum velocities (filtered to periods longer than 2.0 sec) exceed 1.0 m/sec over an area of 700 square kilometres. The peak displacements tend to increase along the strike of the fault away from the epicentre until the end of the fault where they decay rapidly with distance. For simulations with surface rupture, a typical ground motion contains a large amplitude shear wave followed by a train of Rayleigh waves with slightly smaller amplitudes. The most severe ground motion occurs in the direction normal to the fault.

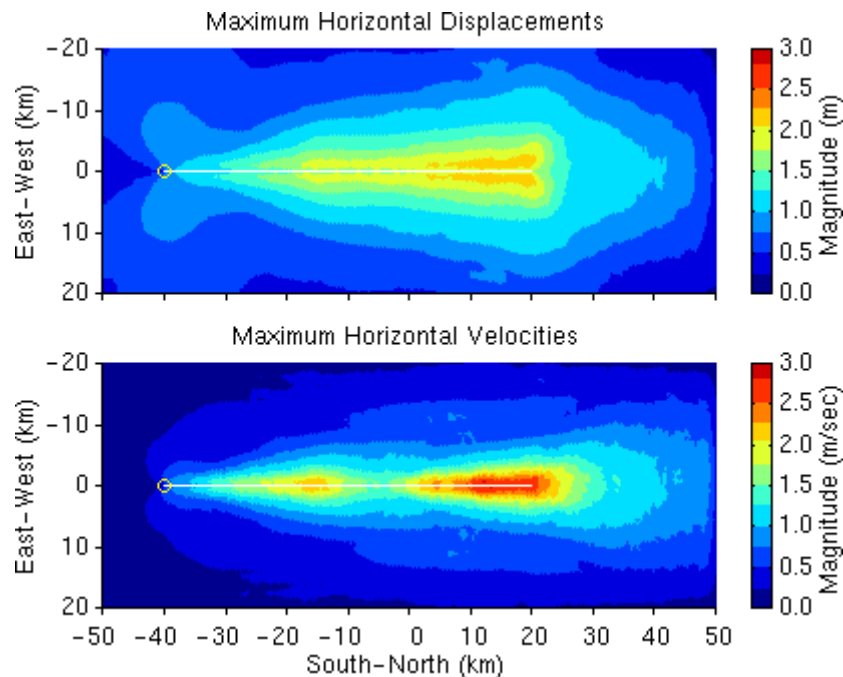


Figure 2: Maximum magnitude of the horizontal displacement and velocity vectors at each point on the ground surface for the base case. The white line indicates the projection of the fault plane on the ground surface, and the yellow circle identifies the epicentre.

Thrust Fault

The thrust fault closely resembles the Elysian Park fault underneath Los Angeles as described by Hall et al. [1995]. The fault measures 28 km long and 18 km wide and dips 23 degrees to the north. We enclose the fault in a domain 60 km long by 60 km wide by 24 km deep as illustrated in figure 3. We impose oblique slip with a rake angle of 105 degrees from the strike to the west to create earthquakes with a nominal moment magnitude of 6.8. We use the same material property variation with depth that we used in the domain with the strike-slip fault. The finite element model contains five million degrees of freedom and eight million elements. The base case features a fault buried 8.0 km below the ground surface with a relatively homogeneous distribution of slip that is tapered on all four edges. We prescribe an average slip of 1.0 m, a maximum slip rate of 1.5 m/sec, a rupture speed of 80% of the local shear wave speed, and a hypocentre at location HA.

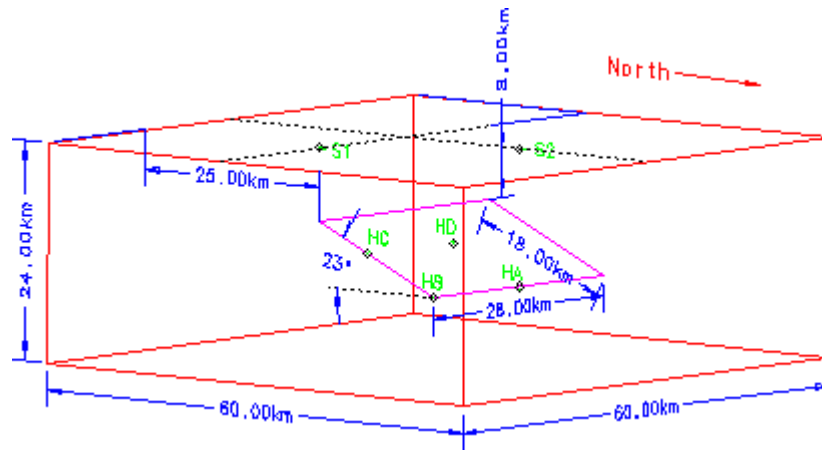


Figure 3: Orthographic view of the geometry of the domain encompassing the thrust fault. The labels HA to HD denote the various hypocentre locations. We examine time histories at sites S1 and S2.

We find several common features in the simulations where the thrust fault is buried 8.0 km below the ground surface. The shallow dip of the fault to the north causes the maximum displacements and maximum velocities (figure 4) to occur 5.0 km south of the top of the fault. The maximum, filtered velocities exceed 1.0 m/sec over an area of 100 square kilometres. The rake angle of 105 degrees directs the largest displacements and velocities towards the Southeast. A large, single pulse in displacement and a corresponding large, double pulse in velocity characterise the ground motions towards the south (the forward direction). The ground motions towards the north (the backward direction) are much less severe. As we raise the top of the fault towards the ground surface, the motion above the fault becomes more severe and a pulse-like shear wave arrival appears in the displacements above the north end of the fault.

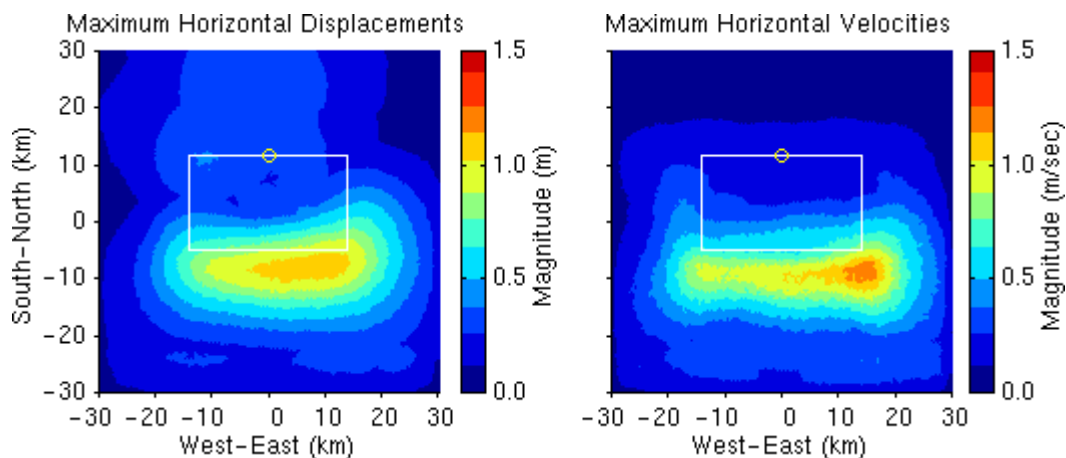


Figure 4: Maximum magnitude of the horizontal displacement and velocity vectors at each point on the ground surface. The white line indicates the projection of the fault plane on the ground surface, and the yellow circle identifies the epicentre.

Assessment of Sensitivity

The ground motions exhibit a strong sensitivity to vertical variation of the material properties (homogeneous half-space versus layered half-space). Softening the material near the surface leads to a substantial increase in the displacement and velocity amplitudes. In the strike-slip simulations at site S1, the peak horizontal displacement increases from 0.40 m to 1.2 m. When we place the top of the fault at the ground surface in the strike-slip simulations, we observe large amplitude Rayleigh waves in the layered half-space but not in the homogeneous half-space. In the thrust fault simulations when we bury the fault beneath the ground surface, the horizontal component dominates the motion in the layered half-space while the horizontal and vertical components are much smaller and roughly the same in the homogeneous half-space.

Increasing the rupture speed compresses the time histories in duration, and we observe a corresponding narrowing of the pulses. Additionally, the reinforcement of the shear wave by the rupture becomes more efficient as the rupture speed increases, because the rupture follows more closely behind the shear wave. This leads to larger amplitudes in both the displacement and velocity time histories in the strike-slip and thrust simulations as we increase the rupture speed from 70% to 90% of the local shear wave speed. In the strike-slip simulations at sites S1 and S2, the peak horizontal velocities increase by 75% and 37%, respectively. However, in the thrust fault simulations this increase is predominantly confined to the horizontal components. The ground motions appear moderately sensitive to variations in the rupture speed.

The ground motions show less sensitivity to changes in the maximum slip rate than they do to changes in the rupture speed. Increasing the maximum slip rate narrows the rupture front which positions the centre of the rupture closer behind the shear wave. As a result, the efficiency of the reinforcement of the shear wave improves, as it does when we increase the rupture speed, and we observe similar increases in the amplitudes of the ground motions. However, on both faults the phases arrive at the same time independent of the maximum slip rate. As illustrated in figure 5, the maximum slip rate influences the amplitude of the motion but not the shapes of the time histories. On the thrust fault increasing the maximum slip rate from 1.0 m/sec to 1.5 m/sec has a greater impact than increasing the maximum slip rate from 1.5 m/sec to 2.0 m/sec.

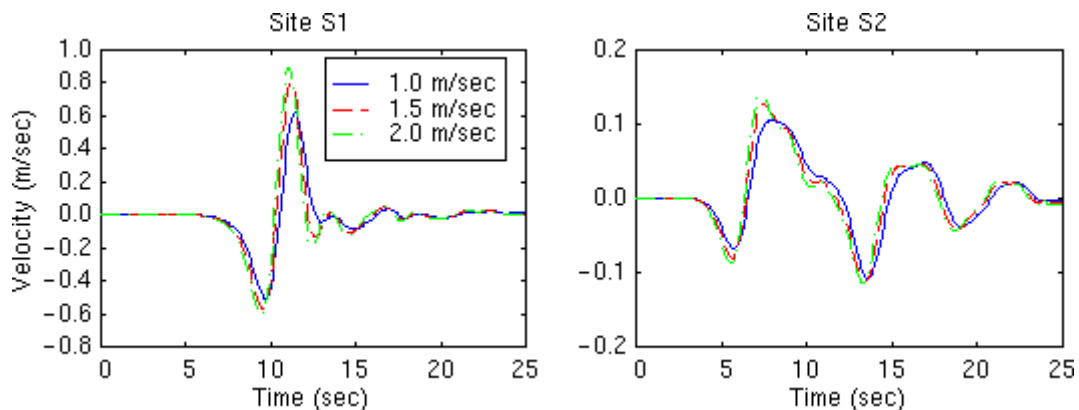


Figure 5: Velocity time histories at sites S1 and S2 for three simulations on the thrust fault with different maximum slip rates. The motion has been rotated into the direction of the maximum horizontal peak to peak velocity.

At a given site the sensitivity of the ground motions to the location of the hypocentre depends on the relative changes in azimuth (angle between the slip vector and the vector from the hypocentre to the site). In the strike-slip simulations the azimuth of the sites in the forward direction remains nearly constant, and we observe very small variations in the motions when we move the hypocentre location. On both faults when the azimuth changes significantly as we move the hypocentre, we find large variations in the ground motions. In some cases, the site may move off of or onto a nodal line, and the ground motions increase or decrease by very large amounts.

The ground motions exhibit little sensitivity to the addition of weak heterogeneity into the distribution of final slip, particularly in the forward direction. However, we expect high frequency ground motion, which we do not include in our simulations, to exhibit a greater sensitivity to heterogeneity in the final slip. In the thrust fault simulations the dip location of the heterogeneity affects the amplitude of the surface waves at sites towards the north (backward direction). In the strike-slip simulations we use a strongly heterogeneous slip distribution which does reduce the displacement amplitudes for a considerable portion of the time history as shown in figure 6. As in the thrust fault simulations with weak heterogeneity, the ground motions in the backward direction show a

greater sensitivity to the strong heterogeneity in the final slip. In the forward direction we do observe some minor changes in the time histories, but the peak displacements and velocities remain relatively unchanged.

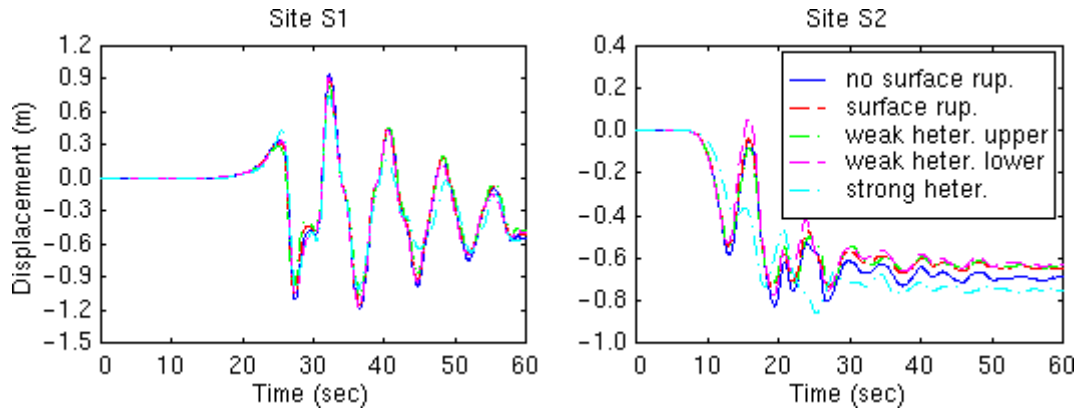


Figure 6: Displacement time histories at sites S1 and S2 for five simulations on the strike-slip fault with different distributions of final slip. The distributions with weak heterogeneity contain a bias towards larger slip on either the upper half of the fault (weak heter. upper) or the lower half of the fault (weak heter. lower). The motion has been rotated into the direction of the maximum horizontal peak to peak velocity.

When we increase the average slip on the fault, the displacement amplitudes increase about the same relative amount as the increase in average slip. For example, increasing the average slip from 1.0 m to 2.0 m on the thrust fault increases the peak horizontal displacement at site S1 by 68% (from 0.95 m to 1.6 m) as shown in figure 7, and the moment magnitude increases from 6.8 to 7.0. Maintaining the same rupture speed and maximum slip rate prevents a similar increase in the velocities; the peak horizontal velocity at site S1 increases by only 19% (from 0.83 m/sec to 0.99 m/sec). The area where the peak velocity exceeds 1.0 m/sec increases from 100 square kilometres to 150 square kilometres. Additionally, by keeping the maximum slip rate the same, the larger slip leads to a longer rise time. Consequently, we observe a slight delay in the peak displacement and velocity amplitudes as we increase the average slip. Thus, the displacements exhibit a strong sensitivity to different values of average slip, while the velocities exhibit a weak sensitivity.

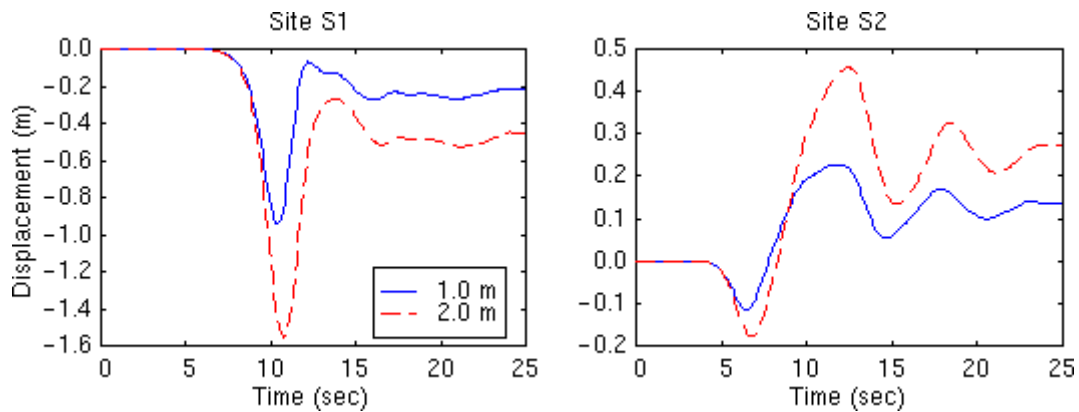


Figure 7: Displacement time histories at sites S1 and S2 for two values of average slip on the thrust fault. The motion has been rotated into the direction of maximum horizontal peak to peak velocity.

In our simulations the ground motions are most severe when the slip occurs near the ground surface. It is interesting to note that raising the top of the fault towards the ground surface while using the same slip distribution shifts the slip to a region with a smaller shear modulus and leads to a slight decrease in the moment magnitude of the earthquake. The moment magnitude decreases from 7.1 to 7.0 as the top of the strike-slip fault moves from a depth of 8.0 km to the ground surface. Similarly, the moment magnitude decreases from 6.8 to 6.6 as we raise the top of the thrust fault to the ground surface from a depth of 8.0 km. While the moment magnitudes decrease, the ground motions become more severe. With shallow slip we observe large amplitude surface waves with several cycles of deformation in addition to the large amplitude shear wave. Raising the top of the thrust fault causes an increase in the motion directly above the fault and shifts the largest motion from south of the top of the fault to directly above the top of the fault. Additionally, the peak maximum horizontal

velocity increases by 50%. On both the strike-slip fault and the thrust fault, the ground motions display a strong sensitivity to the depth of the fault.

DISCUSSION

This sensitivity study shows that in order to accurately model ground motion, in particular ground motion for engineering design, we must carefully select the values of those parameters that cause the most variability in the resulting ground motion. Thus, for a given site we must know the material properties of the surrounding region and the location and geometry of all nearby faults. To simulate the most severe cases of ground motion, the hypocentre should be placed such that the rupture propagates as far as possible towards the site under study and the site lies close to an azimuth of zero. Additionally, we must select reasonable values of the rupture speed, maximum slip rate, and average slip; if the displacement time histories are particularly important, we need to pay special attention to the average slip. As long as the site lies in the forward direction, the spatial distribution of slip on the fault has little influence on the ground motions, so we need not model it with as great of care.

For each group of simulations on the strike-slip fault and the thrust fault, we compare the shapes of the curves of the maximum displacements and maximum velocities along a line running normal to the strike of the fault to the shape of the curve of the Uniform Building Code near-source factor, N_v . If we assume the maximum displacements and velocities correlate with the seismic demand imposed on a building, then we want the shape of the near-source factor curve to match the general shapes of the maximum displacements and the maximum velocities. As we see from figure 8, for the strike-slip fault the near-source factor accurately captures the location of the peak motion and the decay with distance from the fault.

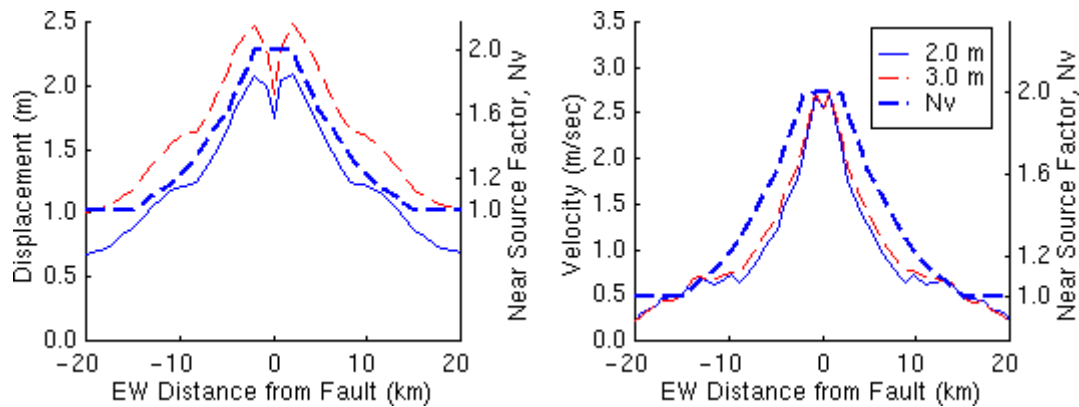


Figure 8: Maximum magnitudes of the horizontal displacement and velocity vectors along an east-west line running through the north tip of the fault for the two values of average slip. The thick, dashed line indicates the near-south ground motion factor, N_v , from the 1997 Uniform Building Code.

We apply the formula for the near-source factor from the 1997 Uniform Building Code to all three depths of the thrust fault. The California Division of Mines and Geology, on the other hand, does not include blind thrust faults on the maps used to determine the near-source factor [California Department of Conservation, 1998]. For the thrust fault the near-source factor is set to a maximum value where the fault lies within 10 km of the surface and 2 km on either side. When we place the fault close to the ground surface, this region does receive the most severe ground motion as shown in figure 9. However, the peak motion falls outside this region when we bury the fault 8.0 km below the surface. The near-source factor remains at a maximum value for only 2.0 km on the up-dip side of the fault regardless of the depth of the top of the fault. In order for the shape of the near-source factor to more closely follow the shapes of the maximum displacements and maximum velocities for blind thrust faults, it must be either shifted towards the up-dip side of the fault or extended in that direction.

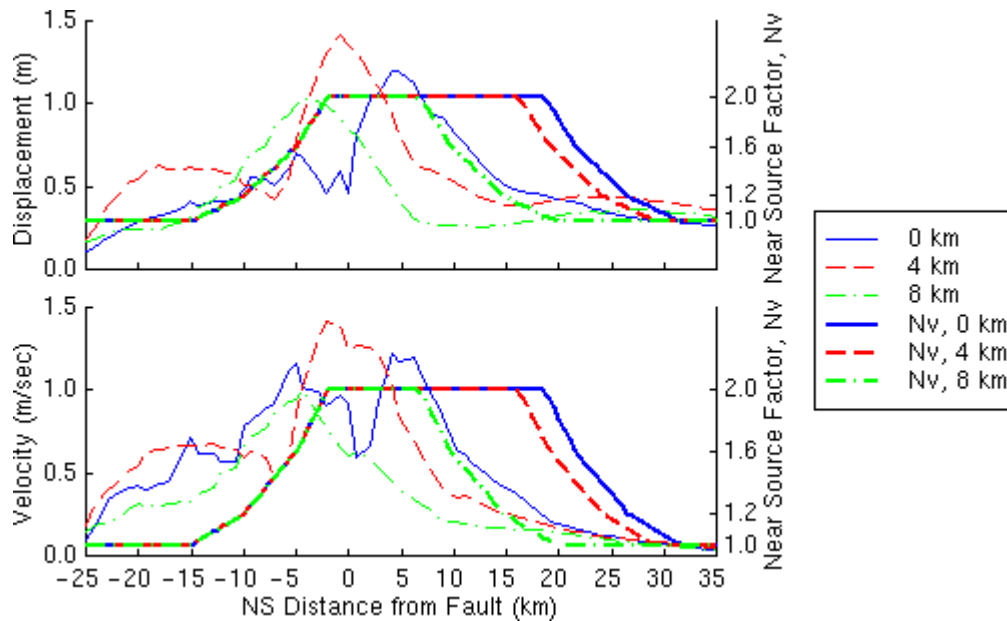


Figure 9: Maximum magnitudes of the horizontal displacement vectors and velocity vectors along a north-south line running through the centre of the fault for the three depths of the top of the fault. The thick lines indicates the near-source ground motion factor, N_v , from the 1997 Uniform Building Code for each of the three depths of the top of the fault.

REFERENCES

- Aagaard, B.T. (1999), "Finite element simulations of earthquakes", Technical Report 99-03, *Earthquake Engineering Research Laboratory, California Institute of Technology*, Pasadena, CA.
- Bao, H.S., Bielak, J. Ghatta, O. Kallivokas, L.F., O'Hallaron, D.R., Shewchuk, J.R., and Xu, J.F. (1998), "Large-scale simulation of elastic wave propagation in heterogeneous media on parallel computers," *Computer Methods in Applied Mechanics and Engineering*, Vol. 152, No. 1-2, pp 85-102.
- Brune, J.N. (1970), "Tectonic stress and spectra of seismic shear waves from earthquakes," *Journal of Geophysical Research*, Vol. 75, pp 4997-5009.
- California Department of Conservation, Division of Mines and Geology (1998), *Maps of known active fault near-source zones in California and adjacent portions of Nevada : to be used with the 1997 uniform building code*, in cooperation with Structural Engineers Association of California, Seismology Committee, International Conference of Building Offices, Whittier, California.
- Cohen, M. (1980), "Silent boundary conditions for transient wave analysis," Technical Report 80-09, *Earthquake Engineering Research Laboratory, California Institute of Technology*, Pasadena, CA.
- Hall, J.F. Heaton T.H., Halling M.W., and Wald, D.J. (1995), "Near-source ground motion and its effects on flexible buildings," *Earthquake Spectra*, Vol. 11, No. 4, pp 569-605.
- Heaton, T.H. (1995), "Overview of seismological methods for the synthesis of strong ground motion," *Proceedings: Modeling Earthquake Ground Motion at Close Distances*, Research Project 3102-04, Electric Power Institute, Palo Alto, CA.
- Rao, S.S. (1999), *The Finite Element Method in Engineering*, Butterworth Heinemann, Boston, 3rd edition.
- Williams, R.D. (1991), "Performance of dynamic load balancing algorithms for unstructured mesh calculations," *Concurrency-Practice and Experience*, Vol. 3, No. 5, pp 457-481.